



Combustion-aminolysis synthesis and characterization of CrN/Cu composites

Aimin Chu^{*1}, Yuping Zhao², Rafi ud-din³, Li Tian¹, Shibo Guo¹, Hongmei Xu¹, Huajian Zhang¹

¹Hunan Provincial Key Defense Laboratory of High Temperature Wear-resisting Materials and Preparation Technology, School of Materials Science and Engineering, Hunan University of Science and Technology, Xiangtan, China.

²School of Civil and Engineering, Hunan University of Science and Technology, Xiangtan, China.

³Materials Division, PINSTECH, Post Office Nilore, Islamabad, Pakistan.

Received: 25 February 2020; Accepted: 20 June 2020

* Corresponding author email: chuaiminme@163.com

ABSTRACT

CrN/Cu composite powders were synthesized by employing a novel two-step technique. Firstly, the Cr₂O₃+CuO precursors were prepared by the solution combustion synthesis (SCS) method using cupric nitrate, urea, and chromium nitrate as initial materials. Subsequently, the SCS precursors were calcined at 850 °C in NH₃ for 6 h, and transformed to CrN/Cu composite powders. The composite powders consist of the uniform subsphaeroidal particles with the particle size ranging from 200 to 300 nm. After the friction-wear test, the removal volume of the sintered CrN/Cu composite specimen (0.0218 mm³) is almost 80 times smaller than that of the sintered pure copper specimen (1.6634 mm³). The addition of CrN can improve the tribological performance of sintered copper significantly. Moreover, the electrical conductivity of the sintered CrN/Cu composite specimen is high to 85.6% of IACS (International Annealed Copper Standard).

Keywords: CrN/Cu composite powder; Precursor; Solution combustion synthesis; Aminolysis; Tribological performance.

1. Introduction

In recent years, copper alloys are extensively employed in chemical, nuclear, thermal, and electrical industries due to their good workability, thermal and electrical conductivities (EC) [1–3]. Excellent resistance to arcing and wear is an essential requirement in various applications such as bushes and nozzles for bearings, electrical contacts. According to the previous reports [4–5], various ceramic particles, including carbides [6], oxides [7], borides [8], nitrides [9] and carbon materials [10–12], can be used as secondary phases to strengthen and improve the sliding wear performance of copper alloys. Bagheri, et al. [6] have investigated the effect of titanium carbide (TiC) particles on

the wear behavior of copper matrix composites (CMCs). They found that the wear resistance has been improved significantly with the addition content of TiC below 5 vol.%. Saravanakumar, et al. [9] have reported that the wear rate of AlN/Cu CMCs decreases with an increase in AlN contents. Wang, et al. [12] have shown the carbon nanotubes CMCs and they exhibit a peak hardness of 1.3 GPa with good mechanical performance.

Excepted for the outstanding mechanical properties, good EC of CMCs is also an essential requirement for their applications. Most current researches have showed that the mechanical properties of copper matrix composites (e.g., hardness, specific strength and specific elastic

modulus) have been improved incredibly by incorporation of intrinsically hard ceramics [6–12]. Whereas, the EC of CMCs drops off considerably at the same time [6, 8]. For a good compatibility between wear property and EC, the appropriate reinforcement should be selected and adopted. Chromium nitride (CrN) is an appropriate choice as the reinforcement for copper matrix composites owing to its wear resistance, high EC, superior corrosion and excellent chemical stability [13]. These properties of CrN along with its inertness to the based materials made it as one of the most promising candidates in enhancing the mechanical properties and EC of copper matrix composites. Therefore, reinforcing copper with CrN is considered to achieve reasonably high wear resistance and maintain good EC in electrical and electronic components synchronously.

The raw powders with fine granularity, good sinterability, and high purity are essential for obtaining the products with good properties. Various experimental techniques are available in literature to prepare the copper matrix composite powders, such as powder metallurgy [14–15], mechanical alloying [6–16], combustion synthesis [17], etc. As well known, the solution combustion synthesis method (SCS) is one of the most appropriate methods to prepare the oxide-based materials [18–19]. In the present study, a novel two-step method, the combined method of SCS and aminolysis has been successfully applied to prepare the CrN/Cu composite powder. Firstly, the $\text{Cr}_2\text{O}_3+\text{CuO}$ precursors were fabricated by the SCS method using $\text{Cr}(\text{NO}_3)_3$, $\text{Cu}(\text{NO}_3)_2$, and $\text{CO}(\text{NH}_2)_2$ as the starting materials. Then, the CrN/Cu composite powders were prepared by the aminolysis of SCS precursor. Tribological performance of the sintered pure copper powder and CrN/Cu composite powder specimens, whose raw powders were prepared by the same SCS and aminolysis synthesis methods, was investigated and compared in detail.

2. Experimental details

2.1. Starting materials

The $\text{Cr}_2\text{O}_3+\text{CuO}$ precursors were fabricated by the SCS method using $\text{Cu}(\text{NO}_3)_2$ and $\text{Cr}(\text{NO}_3)_3$ as the oxidizer and $\text{CO}(\text{NH}_2)_2$ as the reducer. The optimal molar ratio of $\text{CO}(\text{NH}_2)_2$ to $\text{Cu}(\text{NO}_3)_2$ (U/Cu) in the solution is 2:1 and the concentration of $\text{Cu}(\text{NO}_3)_2$ is 0.1 mol/L. For a comparative study, the concentrations of $\text{Cr}(\text{NO}_3)_3$ in the two initial

solutions were set as 0 mol/L and 0.005 mol/L to evaluate the effect of CrN on the properties of the final sintered CrN/Cu composite powder specimens.

2.2. Synthesis procedure

The detailed synthesis procedure for the SCS precursors was mentioned in our previous research [20]. Then, the two precursors were calcined at 850 °C for 6 h in ammonia atmosphere with a flow rate of 0.5 L/min to obtain the pure Cu and CrN/Cu composite powders. Subsequently, two kinds of the as-prepared powders were sintered at 775 °C for 5 min under the pressure of 30 MPa by spark plasma sintering (SPS) to obtain the sintered specimens.

2.3. Characterization

XRD patterns of the SCS precursors and the calcined powders were acquired on an X-ray diffractometer using a radiation of CuK_α (Rigaku, D/max-RB12). The granularity and morphology of the precursors and the calcined powders were observed by field emission scanning electron microscopy (FE-SEM, JSM-6701F). The morphologies of the worn surfaces for the sintered pure copper and CrN/Cu composite samples were observed by scanning electron microscopy (SEM, JSM-6301F) equipped with energy dispersive spectrometer (EDS, OXFORD Link-ISIS-300). The specific surface area (SSA) of the precursors and the calcined powders was tested using an Automated Surface Area & Pore Size Analyzer (QUADRASORB SI-MP). Vickers hardness of the sintered samples was tested using a HV-30 tester by applying a load of 294.2 N for 20 s and took an average value of twelve measurements. The theoretical density was calculated from the sample rule of mixtures and the experimental density was determined by the Archimedes method. The relative density is the ratio of the experimental and theoretical densities of the sintered samples. The EC of the sintered samples was measured using an eddy current conductivity meter (Sigma 2008, USA).

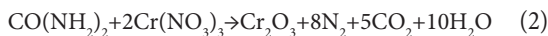
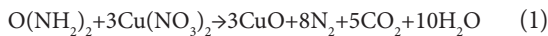
To investigate the tribological performance of the sintered specimens in air, the friction tests were carried out on a high-speed reciprocating friction and wear tester (HSR-2M). The samples were kept stationary by a high-strength metal disk. The counterface ball is a steel ball with a diameter of 4 mm (60 HRC) which maintained a sliding distance of 5 mm in the reciprocation motion. The applied load and duration were 10 N and 20 min,

respectively, and the sliding speed was 0.1 m/s during the friction test.

3. Results and discussion

3.1. Preparation of the SCS precursors

The XRD pattern of the precursor prepared from $\text{Cr}(\text{NO}_3)_3$ with a concentration of 0.005 mol/L in the solution is shown in Fig. 1. It is clear from Fig. 1 that only the diffraction peaks of CuO (JCPDS card 44-0706) and Cr_2O_3 (JCPDS card 38-1479) are visible, implying the complete transformations of $\text{Cu}(\text{NO}_3)_2$ to CuO and $\text{Cr}(\text{NO}_3)_3$ to Cr_2O_3 during combustion reaction, which can be expressed by the reaction equations (1) and (2), respectively.



The various ΔG of the reactions (1) and (2) with respect to the temperature are shown in Table 1. All the thermodynamic data were obtained from the JANAF tables [21]. It is clear that the ΔG of the reactions (1) and (2) is below zero at 298~1073 K, implying that the reactions (1) and (2) would go spontaneously to the right of the reaction equations during the combustion reaction. However, the temperature of the solutions at 573 K is enough to

cause the reactions (1) and (2) to happen.

Fig. 2 shows the FE-SEM images of the precursor prepared from prepared from $\text{Cr}(\text{NO}_3)_3$ with a concentration of 0.005 mol/L in the solution. It is clear that the precursor is comprised of large particles with tens of microns in size and exhibits a polyporous structure (Fig. 2a), which are the result from the clustering of small spherical particles with a size up to $\sim 1 \mu\text{m}$ (Fig. 2b). The specific surface area of this precursor is $5.8 \text{ m}^2/\text{g}$, which is owing to the dispersant effect of gases generated during the combustion process [22].

3.2. Preparation of the calcined powders

Subsequently, the precursor is calcined at 850°C in ammonia for 6 h. Fig. 3 presents the XRD pattern of the calcined powders. It is clear that the CrN/Cu composite powders exhibit the diffraction peaks of CrN (JCPDS card 11-0065) and Cu (JCPDS card 04-0836), implying the transformations of CuO to Cu and Cr_2O_3 to CrN according to the reactions (3) and (4) during calcination, respectively. Obviously, the CrN/Cu composite powders can be obtained by using the SCS and aminolysis method. The various ΔG of the reactions (3) and (4) with the respect to the temperature are shown in Table 1. It is clear that the ΔG of the reactions (3) and (4) are equal to zero

Table 1- ΔG of various reactions at different temperatures

T/K	(1)	(2)	(3)	(4)
298	-326.5	-232.3	76.7	145.6
421	-528.7	-426.4	0	55.8
617	-762.1	-632.3	-372.5	0
1073	-1032.9	-852.8	-544.6	-486.5

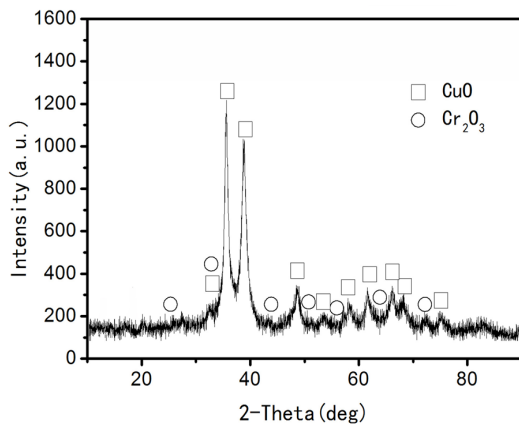


Fig. 1- XRD pattern of the precursor prepared from $\text{Cr}(\text{NO}_3)_3$ with a concentration of 0.005 mol/L in the solution.

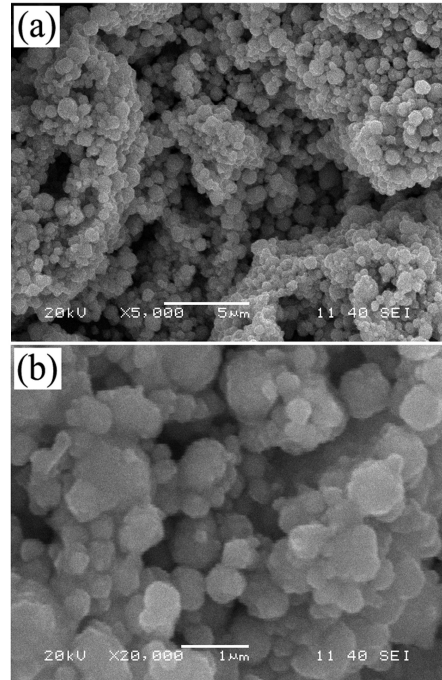


Fig. 2- FESEM images ((a) 5 KX; (b) 20 KX) of the precursor prepared from $\text{Cr}(\text{NO}_3)_3$ with a concentration of 0.005 mol/L in the solution.

at the critical temperatures (T^*) of 421 K and 617 K, respectively, implying that the reactions (3) and (4) will go spontaneously to the right of the reaction equations at the temperature above T^* . However, the temperature of the systems at 1073 K is enough to cause the reactions (3) and (4) to occur.



Fig. 4 presents the FESEM images of the CrN/Cu composite powders. Compared to the large particles in the precursor, the prepared CrN/Cu composite powders consist of numerous subsphaeroidal particles with a size of 200 nm to 300 nm (Fig. 4a), and the boundaries among particles are very distinct (Fig. 4b), which indicates that the large particles of the precursor powder (Fig. 2) have transformed into the small fragmentized subsphaeroidal particles (Fig. 4) after calcining at 850 °C in ammonia for 6 h. In addition, the SSA of CrN/Cu composite powders increases from 5.8 m²/g of the corresponding precursor to 11.5 m²/g. In a word, the CrN/Cu

composite powders are obtained so as to prepare the sintered CrN/Cu composite sample with a good anti-wear performance.

3.3. characterization of the sintered pure copper and CrN/Cu composite specimens

Fig. 5 shows the friction coefficient (CoF) of the sintered pure copper and CrN/Cu composite specimens. As shown in Fig. 5, the curve of the friction coefficient (CoF≈0.63) for the pure copper specimen fluctuates greatly, which shows that the pure copper specimen exhibits poor anti-friction performance. Whereas, the average CoF of the sintered CrN/Cu composite specimen is 0.26, which is about 58% lower than that of the reference pure copper specimen. Moreover, the curve of the CoF for the CrN/Cu composite material fluctuates smoothly. These results suggest that the addition of CrN can improve greatly the abrasive resistance of copper.

SEM images of the worn surfaces of the sintered pure copper and CrN/Cu composite specimens are shown in Fig. 6. Obvious changes are observed on

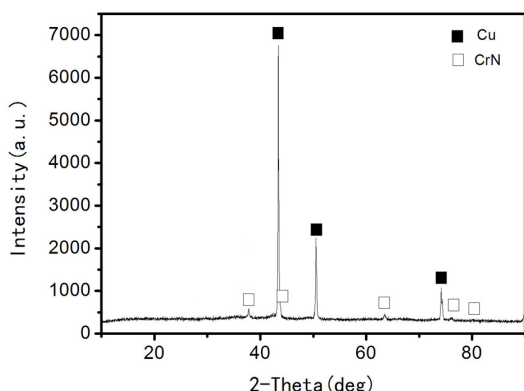


Fig. 3- XRD pattern of the calcined CrN/Cu composite powders.

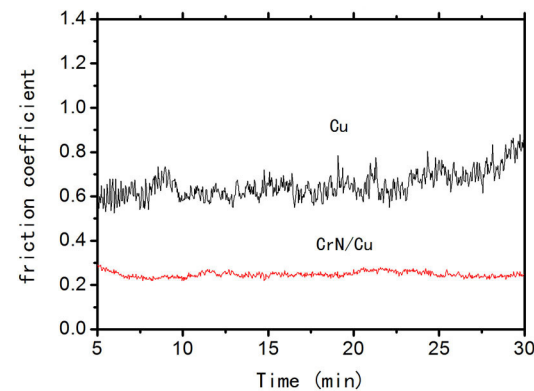


Fig. 5- The friction coefficient of the pure copper and CrN/Cu composite specimens.

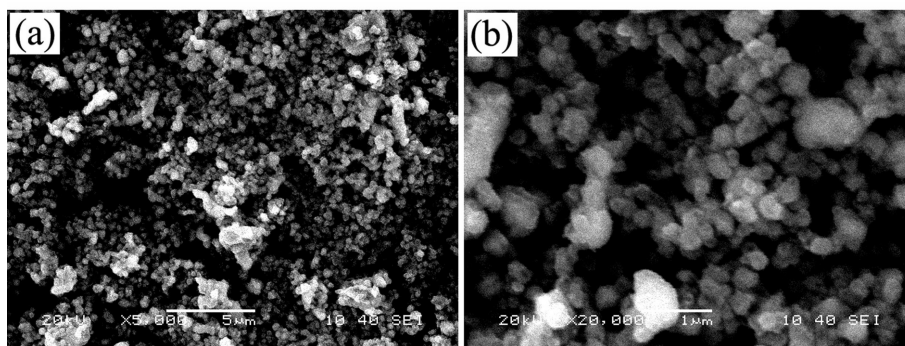


Fig. 4- FESEM images of ((a) 5 KX; (b) 20 KX) of the CrN/Cu composite powders.

the worn surfaces of the specimens reinforced with and without CrN particles. For the pure copper specimen, it can be seen that the subsurface is fully exposed accompanying with significant lots of flaws and large area shedding as shown in Fig. 6a. Moreover, a layer of the red-brown material is attached to the surface of the corresponding steel ball, which indicates that the wear of Cu matrix is serious adhesion wear. This phenomenon is ascribed to the frictional heat evolution during the sliding. This heat causes the thermal softening of copper, producing a large number of debris that results in a large scale of material removal. The wear rate is relatively higher for the pure copper specimen (The removal volume is 1.6634 mm³, as shown in Table 2). The wear mechanism for the pure copper specimen is observed to be the adhesion wear.

However, the sliding wear behavior is considerably improved by the addition of CrN particles in copper. A much smoother worn surface with some grooves can be found for the CrN/Cu

composite specimen (Fig. 6b). The worn surface also exhibits the generation of some wear debris during the sliding test as well as the observed little plastic deformation and few subsurface delamination. These characteristics of worn surface morphology indicate the presences of the slight adhesion wear (indicated by ring in Fig. 6b) and the dominant abrasive wear (indicated by square in Fig. 6b). The well-distributed CrN particles hinder the plastic deformation of copper matrix causing by the frictional heat as well as the formation of craters. Hardness is the comprehensive embodiment of several mechanical properties, such as strength, stiffness, abrasion resistance, etc [23]. The values of vickers hardness for the pure copper and CrN/Cu composite specimens are 76 HV and 127 HV, respectively (Table 2). It is clear that the hardness of copper matrix can be enhanced by the addition of CrN, which results in the decrease in the real area of the worn track. The real area of the worn track is defined as the ratio of the applied load to hardness in this study [6]. Consequently, the wear

Table2- Removal volume of worn surface, vickers hardness, relative density, and electrical conductivity of sintered samples

Specimen	Removal volume (mm ³)	Vickers hardness (HV)	Relative density (%)	Electrical conductivity (%, IACS)
Pure Cu	1.6634	76	99.2	98.2
CrN/Cu	0.0218	127	96.5	85.6

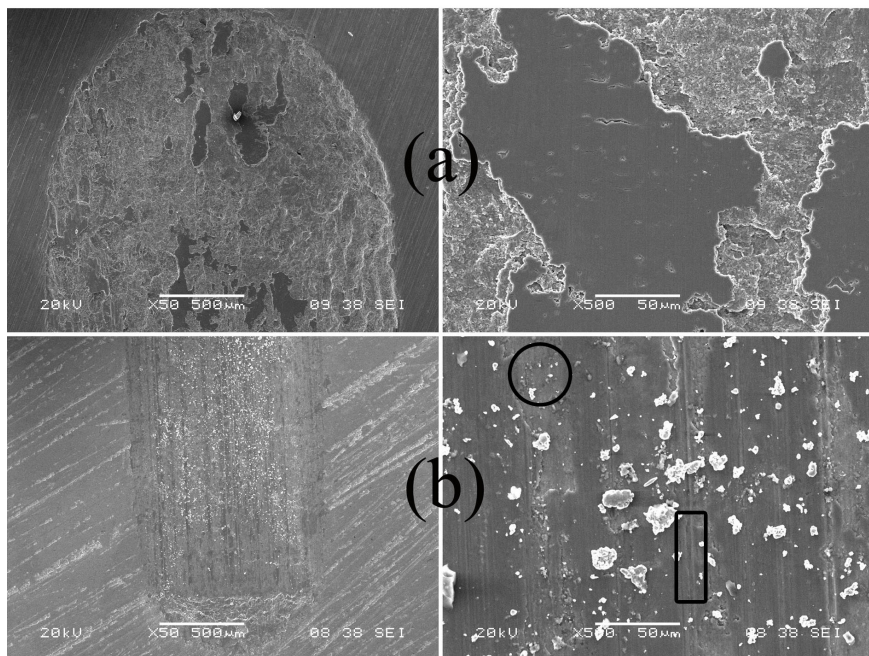


Fig. 6- SEM micrographs of worn surface of the sintered pure copper (a) and CrN/Cu composite (b) specimens.

rate decreases for the CrN/Cu composite specimen. Another possible reason for the improvement of wear resistance is that the CrN particles can bear a part of the applied load and weaken the deformation force on Cu matrix [24]. Therefore, the removal volume of the CrN/Cu composite specimen decreases to 0.0218 mm^3 (Table 2), which is almost 80 times smaller than that of the pure copper specimen. The wear mechanism has transformed from the adhesion wear for the pure copper specimen to the combination of the slight adhesion wear and the dominant abrasive wear for the CrN/Cu composite specimen.

Fig. 7 shows the wear track profiles for the sintered reference pure copper and CrN/Cu composite samples. It is obvious that the depth of the wear track of the reference pure copper sample is 20 times deeper than that of the CrN/Cu composite sample, implying that the anti-wear performance of the pure copper is improved by the addition of CrN particles evidently.

The electrical conductivities (EC) of the sintered reference pure copper and CrN/Cu composite samples were also measured by the eddy-current method, as summarized in Table 2. It is obvious from Table 2 that the EC of the

sintered pure copper sample is 98.2% of IACS and not completely reaches 100% of IACS. The slight variation in the EC of the sintered reference pure copper can be related with the incomplete dense (The relative density is 99.2% as shown in Table 2). Fig. 8 presents the FESEM images of the fractured surfaces of the sintered reference pure copper and CrN/Cu composite samples. It is clear in Fig. 8a that some holes present on the fractured surfaces of the sintered reference pure copper, which is the main reason for the incomplete dense (99.2%) and the decreased EC. The EC of the Cu composites depends on the volume fraction and dispersion extent of the additive, the EC of the additive and Cu matrix, and the interface between the additive and Cu in composites [12]. Compared to the reference pure copper sample, with the addition of CrN, the drops of the EC and relative density (85.6% of IACS and 96.5% as given in Table 2, respectively) are due to the production of defects in the CrN/Cu composites, such as the agglomeration of the CrN particles, the interfaces between Cu and CrN, and pores, as shown in Fig. 8b.

However, the agglomeration of CrN particles is rare, as shown in Fig. 8b. The component of these agglomerated CrN particles was verified by

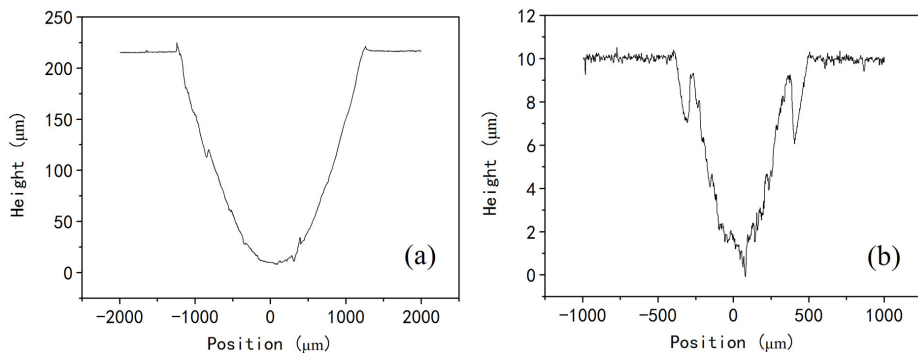


Fig. 7- Cross-sectional profiles of the wear tracks of the sintered pure Cu (a) and CrN/Cu composite (b) samples.

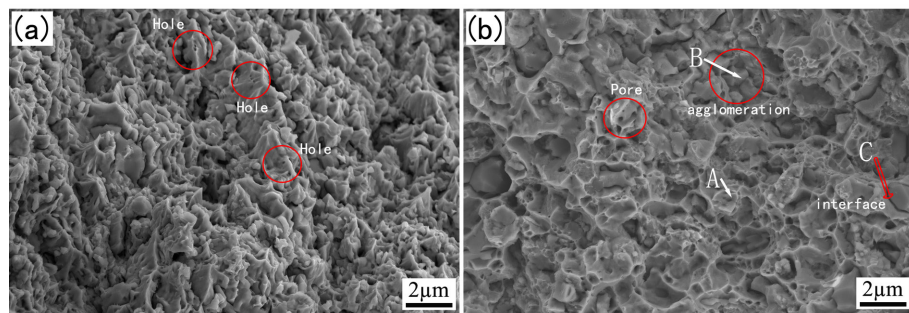


Fig. 8- FESEM photographs of the fractured surfaces of the sintered pure Cu (a) and CrN/Cu composite (b) samples.

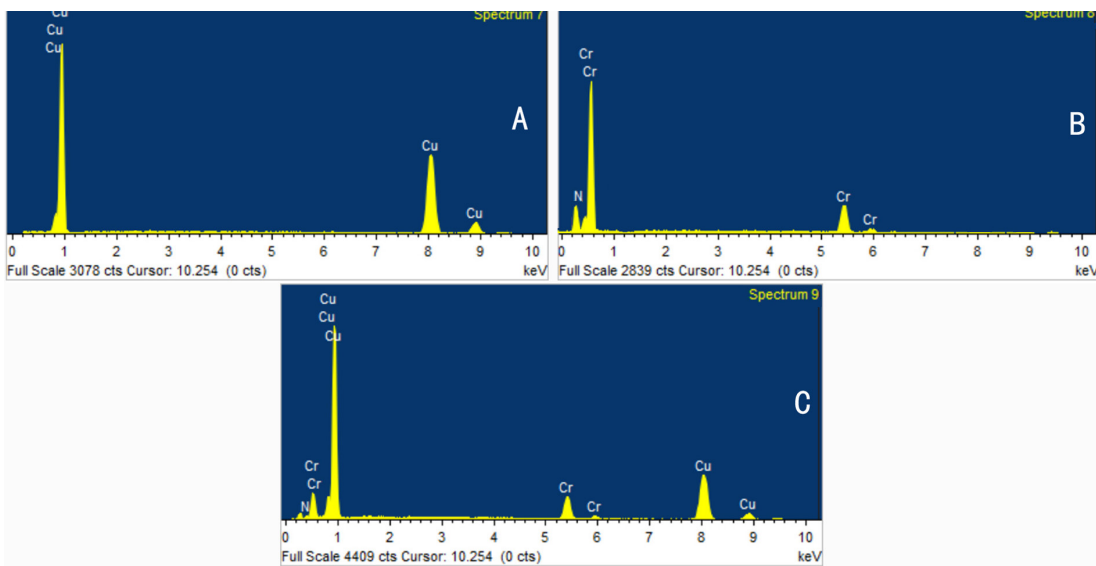


Fig. 9- EDS results of the corresponding areas in Fig. 8b.

EDS, as shown in Fig. 9B. Two kinds of measures may be adopted to avoid the agglomeration of CrN particles, for example reducing the amount of adding CrN, and utilizing some rapid heating ways such as the microwave heating to realize quick solution combustion so as to prevent the component segregation. It is also obvious in Fig. 8b that there are still some interfaces between the Cu matrix and CrN particles on the fractured surfaces of the CrN/Cu composite samples. The EDS result of the interfaces between the Cu matrix and CrN particles is shown in Fig. 9C. Moreover, it is clear in Fig. 8b that there are some subsphaeroidal holes with submicron level existed uniformly in Cu matrix (see EDS result of Fig. 9A), whose distribution nearly agrees with that in the sintered reference pure copper sample (Fig. 8a). These holes may be due to the generated gas according to reaction (5), in which CuO comes from the slight oxidation of nanometer Cu powder due to the high activity during preparing the samples. However, the comprehension about the formation mechanism for these holes in the two sintered samples is still under investigation and will be published later.



Finally, relatively speaking, the EC of the CrN/Cu composites still maintains at a high level (85.6% of IACS). Therefore, according to the results above, CrN can be considered to be a proper choice as the reinforcement for copper matrix in view of the

good compatibility between the wear performance and EC.

4. Conclusions

CrN/Cu composite powders are successfully prepared by a novel SCS and aminolysis route. The SCS precursor particles are comprised of CuO and Cr₂O₃ and exhibit a poly porous and large structure. It is also observed that, after the calcination at 850 °C in ammonia for 6 h, the large precursor particles have transformed into the small fragmentized subsphaeroidal CrN/Cu composite particles. Vickers hardness for the sintered CrN/Cu composite specimen (127 HV) is 67% higher than that for the pure copper specimen (76 HV). The average CoF of the sintered CrN/Cu composite (CoF≈0.26) is much smaller than that of the pure copper (CoF≈0.63). The wear track of the pure copper sample is 20 times deeper than that of the CrN/Cu composite sample. The wear mechanism has changed from the adhesion wear for the pure copper specimen to the combination of the slight adhesion wear and the dominant abrasive wear for the CrN/Cu composite specimen. Undoubtedly, the addition of CrN particles can improve the wear resistance performance of copper evidently and maintains the EC of CrN/Cu composites at a high level (85.6% of IACS).

5. Funding

This work is financially supported by Scientific Research Fund of Hunan Provincial Education

Department (18A196 and 14B065), Natural Science Foundation Program of Hunan (2017JJ2091) and National Natural Science Foundation Program of China (51675176).

references

1. Rajkumar K, Aravindan S. Microwave sintering of copper-graphite composites. *Journal of Materials Processing Technology*. 2009;209(15-16):5601-5.
2. Koppad PG, Aniruddha Ram HR, Kashyap KT. On shear-lag and thermal mismatch model in multiwalled carbon nanotube/copper matrix nanocomposites. *Journal of Alloys and Compounds*. 2013;549:82-7.
3. Fathy A, Shehata F, Abdelhameed M, Elmahdy M. Compressive and wear resistance of nanometric alumina reinforced copper matrix composites. *Materials & Design* (1980-2015). 2012;36:100-7.
4. Jha P, Gautam RK, Tyagi R, Kumar D. Sliding Wear Behavior of TiC-Reinforced Cu-4 wt% Ni Matrix Composites. *Journal of Materials Engineering and Performance*. 2016;25(10):4210-8.
5. Chen Q, Li DY, Cook B. Is porosity always detrimental to the wear resistance of materials?—A computational study on the effect of porosity on erosive wear of TiC/Cu composites. *Wear*. 2009;267(5-8):1153-9.
6. Bagheri GA. The effect of reinforcement percentages on properties of copper matrix composites reinforced with TiC particles. *Journal of Alloys and Compounds*. 2016;676:120-6.
7. Fathy A, Megahed AA. Prediction of abrasive wear rate of in situ Cu-Al₂O₃ nanocomposite using artificial neural networks. *The International Journal of Advanced Manufacturing Technology*. 2011;62(9-12):953-63.
8. Sharma AS, Mishra N, Biswas K, Basu B. Fretting wear study of Cu-10wt% TiB₂ and Cu-10wt% TiB₂-10wt% Pb composites. *Wear*. 2013;306(1-2):138-48.
9. Saravanakumar S, Gopalakrishnan S, Dinaharan I, Kalaiselvan K. Assessment of microstructure and wear behavior of aluminum nitrate reinforced surface composite layers synthesized using friction stir processing on copper substrate. *Surface and Coatings Technology*. 2017;322:51-8.
10. Chen F, Ying J, Wang Y, Du S, Liu Z, Huang Q. Effects of graphene content on the microstructure and properties of copper matrix composites. *Carbon*. 2016;96:836-42.
11. Yue H, Yao L, Gao X, Zhang S, Guo E, Zhang H, et al. Effect of ball-milling and graphene contents on the mechanical properties and fracture mechanisms of graphene nanosheets reinforced copper matrix composites. *Journal of Alloys and Compounds*. 2017;691:755-62.
12. Wang H, Zhang Z-H, Zhang H-M, Hu Z-Y, Li S-L, Cheng X-W. Novel synthesizing and characterization of copper matrix composites reinforced with carbon nanotubes. *Materials Science and Engineering: A*. 2017;696:80-9.
13. García-Márquez A, Portehault D, Giordano C. Chromium nitride and carbide nanofibers: from composites to mesostructures. *J Mater Chem*. 2011;21(7):2136-43.
14. Balamurugan P, Uthayakumar M. Influence of Process Parameters on Cu-Fly Ash Composite by Powder Metallurgy Technique. *Materials and Manufacturing Processes*. 2015;30(3):313-9.
15. Ponraj NV, Azhagurajan A, Vettivel SC, Sahaya Shajan X, Nabhiraj PY, Sivapragash M. Graphene nanosheet as reinforcement agent in copper matrix composite by using powder metallurgy method. *Surfaces and Interfaces*. 2017;6:190-6.
16. Sheibani S, Ataie A, Heshmati-Manesh S. In-Situ Synthesis of Cu/Cr-Al₂O₃ Nanocomposite by Mechanical Alloying and Heat Treatment. *Metallurgical and Materials Transactions A*. 2010;41(10):2606-12.
17. Lu J, Shu S, Qiu F, Wang Y, Jiang Q. Compression properties and abrasive wear behavior of high volume fraction TiCx-TiB₂/Cu composites fabricated by combustion synthesis and hot press consolidation. *Materials & Design*. 2012;40:157-62.
18. Kingsley JJ, Patil KC. A novel combustion process for the synthesis of fine particle α -alumina and related oxide materials. *Materials Letters*. 1988;6(11-12):427-32.
19. Chu A, Guo Z, Ud-din R, Dong Y, Wang L, Liu W, et al. Effect of fuel type on the aminolysis synthesis of CrN powders from combustion synthesis precursors. *Advanced Powder Technology*. 2018;29(6):1439-44.
20. Chu A, Wang Z, Rafi ud d, Dong Y, Guo C, Liu W, et al. Citric acid-assisted combustion-nitridation-denitridation synthesis of well-distributed W-Cu nanocomposite powders. *International Journal of Refractory Metals and Hard Materials*. 2018;70:232-8.
21. Frurip DJ, Syverud AN, Chase MW. Thermodynamic properties of diatomic gases at high temperatures: An improved calculational approach for the JANAF thermochemical tables. *Journal of Nuclear Materials*. 1985;130:189-98.
22. Cao Z, Qin M, Zuo C, Jia B, Liu Y, Gu Y, et al. Effect of glycine on the synthesis of CrN nanopowder using nitridation combustion synthesis precursors. *Journal of Nanoparticle Research*. 2015;17(2).
23. Nieto A, Bisht A, Lahiri D, Zhang C, Agarwal A. Graphene reinforced metal and ceramic matrix composites: a review. *International Materials Reviews*. 2016;62(5):241-302.
24. Shi Z, Yan M. The preparation of Al₂O₃-Cu composite by internal oxidation. *Applied Surface Science*. 1998;134(1-4):103-6.